AD-A138 245 ACOUSTIC EXPLORATION OF OCEAN FLOOR PROPERTIES BASED ON 1/1
THE RINGING OF SE..(U) CATHOLIC UNIV OF AMERICA
WASHINGTON DC DEPT OF PHYSICS A NAGL ET AL. 30 NOV 83
UNCLASSIFIED N00014-76-C-0430 F/G 20/1 NL

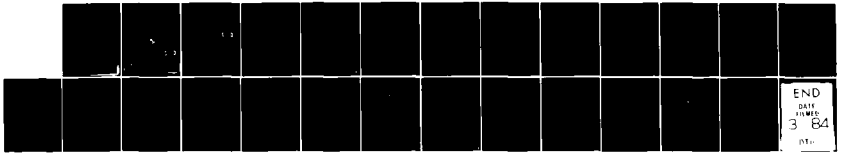

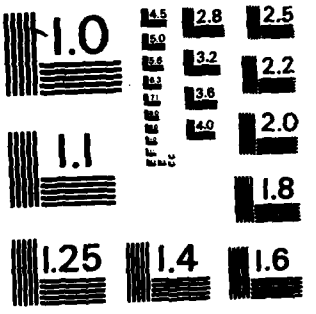

MICROCOPY RESOLUTION TEST CHART
NATIONAL BUREAU OF STANDARDS-1963-A

12

ACOUSTIC EXPLORATION OF OCEAN FLOOR PROPERTIES BASED ON THE RINGING OF SEDIMENT LAYER RESONANCES

Anton Nagl, Herbert Überall, and Kwang-Bock Yoo
Department of Physics
Catholic University of America
Washington, DC 20064[1]

DEPARTMENT OF PHYSICS

The Catholic University of America
Washington, D.C. 20064

ACOUSTIC EXPLORATION OF OCEAN FLOOR PROPERTIES BASED ON THE RINGING OF SEDIMENT LAYER RESONANCES

Anton Nagl, Herbert Überall, and Kwang-Bock Yoo
Department of Physics
Catholic University of America
Washington, DC 20064[1]

Abstract

It has recently been shown that the physical properties of a layered ocean floor may in principle be determined from an analysis of the resonances in frequency, or in the angle of incidence, which appear in bottom-reflected acoustic signals. In the present paper we demonstrate how, using sinusoidal signals of long but finite duration, individual resonances can be selectively excited and analyzed. Multiple-bounce layer resonances interfere destructively with the specular echo, and manifest themselves through a characteristic ringing.

---

1 Part of this work was carried out while the authors were visitors to the College of Marine Studies, University of Delaware, DE 19958.

Unclassified

SECURITY CLASSIFICATION OF THIS PAGE (When Data Entered)

REPORT DOCUMENTATION PAGE		READ INSTRUCTIONS BEFORE COMPLETING FORM
1. REPORT NUMBER	2. GOVT ACCESSION NO. AD-A138245	3. RECIPIENT'S CATALOG NUMBER
4. TITLE (and Subtitle) Acoustic Exploration of Ocean Floor Properties based on the Ringing of Sediment Layer Resonances.		5. TYPE OF REPORT & PERIOD COVERED Technical Report (Interim) Oct.1,1982-Sept.30,1983
		6. PERFORMING ORG. REPORT NUMBER
7. AUTHOR(s) A. Nagl, H. Überall and K. B. Yoo		8. CONTRACT OR GRANT NUMBER(s) ONR N00014-76-C-0430
9. PERFORMING ORGANIZATION NAME AND ADDRESS Department of Physics Catholic University Washington, DC 20064		10. PROGRAM ELEMENT, PROJECT, TASK AREA & WORK UNIT NUMBERS Project PR011-08-01 Work Unit NR384-914
11. CONTROLLING OFFICE NAME AND ADDRESS Office of Naval Research Physics Program Arlington, VA 22217		12. REPORT DATE November 30, 1983
		13. NUMBER OF PAGES 16pp.+7ppfigs.+1pform 1473
14. MONITORING AGENCY NAME & ADDRESS(if different from Controlling Office)		15. SECURITY CLASS. (of this report) Unclassified
		15a. DECLASSIFICATION/DOWNGRADING SCHEDULE

16. DISTRIBUTION STATEMENT (of this Report)

Approved for public release; distribution unlimited.

17. DISTRIBUTION STATEMENT (of the abstract entered in Block 20, if different from Report)

18. SUPPLEMENTARY NOTES

19. KEY WORDS (Continue on reverse side if necessary and identify by block number)

Acoustic Reflection, Ocean Bottom, Resonances, Bottom Properties, Transients.

20. ABSTRACT (Continue on reverse side if necessary and identify by block number)

It has recently been shown that the physical properties of a layered ocean floor may in principle be determined from an analysis of the resonances in frequency, or in the angle of incidence, which appear in bottom-reflected acoustic signals. In the present paper we demonstrate how, using sinuosoidal signals of long but finite duration, individual resonances can be selectively excited and analyzed. Multiple-bounce layer resonances interfere destructive with the specular echo, and manifest themselves through a characteristic ringing.

DD FORM 1 JAN 73 1473 EDITION OF 1 NOV 65 IS OBSOLETE S/N 0102-LF-014-6601

Unclassified

SECURITY CLASSIFICATION OF THIS PAGE (When Data Entered)

1. Introduction

Remote acoustic sensing of the ocean floor conventionally employs pulse arrival time methods [see, e.g., Houtz, 1974; Bell and Porter, 1974; Maynard et al., 1974], which permit a determination of the ocean floor depth profile and, to some extent, also of the thicknesses and sound velocities of sediment layers but not of the layer densities. We recently proposed a new method for the remote sensing of ocean floor properties [Nagl, Überall and Hoover, 1982] which, at least in principle, may lead to a determination of all layer parameters by remote acoustic sensing, provided the layer structure is well defined. This method is based on analyzing the effects of layer resonances which are carried by acoustic signals reflected from the ocean floor; and as shown by us, it relates measured resonances parameters (locations, heights, widths) explicitly to the medium parameters (densities, thicknesses, sound velocities etc. of the layers), hence providing a solution to the inverse scattering problem.

In the mentioned reference [Nagl, Überall, and Hoover, 1982], the steady-state reflections of purely sinusoidal signals were considered, as applied to the case of a fluid layer sandwiched between two different fluid half-spaces with the impedances increasing with depth, this case being the simplest model relevant to a sediment-covered ocean floor. Using the same model, we here study the implications of employing finite-length sinusoidal wave trains as acoustic probes. These enable us to directly study individual layer resonances and to observe their ringing, thus directly measuring the resonances width. Furthermore, they permit a separation of the reflected signal into a specularly reflected component, and one

that has undergone multiple reflections within the layer, as well as a determination of the interference between the two components. Consequently, more information is obtained from the use of finite-length wave trains rather than of steady-state sinuosoids. In fact, it will be shown that in principle two long wave-trains reflected at different angles contain enough information to permit a determination of all five bottom parameters in the three-fluid model considered here.

2. The Reflection Coefficient for the Three-Fluid Model

The geometry of the three-fluid model is shown in Fig. 1. Sound is incident through the ocean water (medium 3), reflects from or penetrates the sediment (medium 2), then reflects from or penetrates the substratum (medium 1). The sound speed, density, and propagation direction for the ith medium are designated c_i, p_i, and θ_i, respectively, and d is the thickness of the sediment layer.

The total reflection coefficient, as a function of wave number $k=\omega/c_3$, for the interface between media 2 and 3 is given by [Nagl, Überall and Hoover, 1982]

$$R(k) = \frac{A\cos\delta - i(1-\tau^2)\sin\delta}{S\cos\delta - i(1+\tau^2)\sin\delta} \tag{1a}$$

where

$$\delta = \frac{d\omega}{c_2}\cos\theta_2 , \qquad \tau^2 = \frac{Z_1 Z_3}{Z_2^2} , \tag{1b}$$

$$A = \frac{Z_1 - Z_3}{Z_2} , \qquad S = \frac{Z_1 + Z_3}{Z_2} , \tag{1c}$$

containing the impedance

$$Z_i = c_i \rho_i / \cos\theta_i \tag{1d}$$

of the ith medium. This reflection coefficient may be decomposed into the form

$$R(k) = -R_3 + R_1(1-R_3^2)e^{ikD}\sum_{m=0}^{\infty}(R_1R_3)^m e^{imkD} \tag{2a}$$

where

$$D = \frac{2\delta}{k} = 2d\frac{c_3}{c_2}\cos\theta_2 , \tag{2b}$$

and where

$$R_i = \frac{Z_i - Z_2}{Z_i + Z_2} , \qquad i = 1,3 \tag{2c}$$

are the reflection coefficients of waves propagating in layer 2 and being reflected from the boundaries with the media 1 and 3, respectively. Geometrically, Eq. (2a) corresponds to the multiple-reflection picture shown in Fig. 2. The phase factors exp ikDin Eq. (2a) account for the phase shift introduced by one round-trip bounce in layer 2. Summing Eq. (2a) leads to

$$R(k) = \frac{-R_3 + R_1 e^{ikD}}{1 - R_1R_3 e^{ikD}}$$

$$= \frac{(a-b)\cos\frac{kD}{2} - i(1-ab)\sin\frac{kD}{2}}{(a+b)\cos\frac{kD}{2} - i(1+ab)\sin\frac{kD}{2}} \tag{2d}$$

with $a = Z_1/Z_2$, $b = Z_3/Z_2$, equivalent to Eq. (1a).

In Fig. 3, we plot $|R(k)|^2$ vs. the dimensionless frequency-thickness product fd (where $f = \omega/2\pi$) at a fixed angle of incidence θ_3 (here taken as normal incidence, $\theta_3 = 0^\circ$), for the model parameters

$$\rho_1 = 6.5, \quad \rho_2 = 3.3, \quad \rho_3 = 1.0 \text{ g/cm}^3$$
$$c_1 = 5495, \quad c_2 = 2544, \quad c_3 = 1500 \text{ m/s}. \tag{3}$$

This graph shows "antiresonances" spaced at regular frequency intervals. A similar picture is obtained if $|R|^2$ is plotted vs. θ_3 at fixed k, except that here the (anti)resonances have different width and are non-uniformly spaced. The layer parameters were chosen such as to achieve high impedance contrasts at both interfaces in order to emphasize the resonance characteristics of the reflected signal. If smaller (more commonly encountered) bottom parameters were used, the resonances in Fig. 3 could appear less pronounced, but all results obtained below still apply.

The resonance condition corresponds to the vanishing of the denominator of Eq. (2d)

$$e^{ikD} = 1/R_1 R_3 \tag{4}$$

satisfied by the complex resonance wave numbers

$$k_n^* D = (2n+1)\pi - i\ln(-1/R_1R_3), \qquad R_1R_3<0, \tag{5a}$$

$$k_n^* D = 2n\pi - i\ln(1/R_1R_3), \qquad R_1R_3>0, \tag{5b}$$

whose real parts determine the resonance frequencies ω_n:

$$\omega_n = c_3 \operatorname{Re} k_n^* \equiv c_3 k_n . \tag{5c}$$

At the resonances one thus finds

$$\exp ik_n D = \pm 1, \tag{6a}$$

the sign being determined by the requirement

$$R_1 R_3 \exp ikD_n > 0. \tag{6b}$$

Since in the ocean floor the impedances generally increase with depth ($Z_1 > Z_2 > Z_3$), one has $R_1 > 0$, $R_3 < 0$ and the resonances are found at

$$k_n D = \omega_n D/c_3 = (2n+1)\pi, \quad n = 0, 1, 2, \ldots, \tag{7a}$$

i.e. for

$$\omega_n = (2n+1)\pi c_3 D = \pi c_2 \frac{2n+1}{2d\cos\theta_2}, \tag{7b}$$

or $$f_n = (n+\tfrac{1}{2})\, c_3 / D. \qquad (7c)$$

Applying Snell's law puts the resonances at the values

$$f_n d = \frac{(2n+1)\, c_3}{4\left[(c_3/c_2)^2 - \sin^2\theta_3\right]^{1/2}} \qquad (8a)$$

of the frequency-thickness product.

From Eq. (6a) it is now apparent that at resonance all multiple-bounce terms in R(k), Eq. (2a), add coherently. Remembering that $R_3 < 0$, we obtain the reflection coefficient at resonance:

$$R(k_n) = |R_3| - R_1 \frac{1 - R_3^2}{1 - |R_2 R_3|} \,. \qquad (8b)$$

Here, a large term is subtracted from the specular-reflection component $|R_3|$, leading to the *minima* ("*anti-resonances*") $|R_3(k_n)|^2$ in Fig. 3.

In contrast, the denominator of Eq. (2d) reaches a maximum for exp ikD =1. The associated frequencies

$$f_n' d = \frac{n\, c_3}{2\left[(c_3/c_2)^2 - \sin^2\theta_3\right]^{1/2}} \qquad (8c)$$

lie halfway in between the resonance frequencies. Successive multiple reflections add destructively (with alternating signs) in Eq. (2a), and in the corresponding reflection coefficient

$$R(k_n') = |R_3| + R_1 \frac{1 - R_3^2}{1 + |R_2 R_2|} \qquad (8d)$$

a small term is subtracted from $|R_3|$, leading to the broad maxima in Fig. 3. The resonances at f_n are thus transmission resonances, or anti-resonances in the reflection coefficient, physically characterized by the multiple reflections adding in phase, but their sum interfering destructively with the specular reflection amplitude.

3. The Reflected Signal for Incident Sinusoidal Wave Trains

Finite-length wave trains may be used to separate specularly and multiply-reflected signals, due to the differences in arrival times involved. A sinusoidal wave train of duration $t_p = 2\pi n_0/\omega_0$ (n_0 being the number of cyles in the pulse which we shall assume integer) and carrier frequency $\omega_0 = k_0 c_3$ has the spectrum

$$G(k) = k_0 \frac{e^{ikc_3 t_p} - 1}{k^2 - k_0^2} , \tag{9}$$

peaked around k_0 or f_0 within the intervals of wave number k or frequency f:

$$\Delta K = 2k_0/n_0 , \quad \Delta F = 2f_0/n_0 , \tag{10a}$$

respectively. If now this interval is small compared to the resonance spacing

$$\Delta f = \frac{c_3}{D} = \frac{c_2}{2d\cos\theta_2} = \frac{c_3}{2d[(c_3/c_2)^2 - \sin^2\theta_3]^{1/2}} , \tag{10b}$$

i.e.,

$$2f_0/n_0 \ll c_2/2d\cos\theta_2 , \tag{11a}$$

and if one lets the carrier frequency f_0 coincide with a resonance frequency,

$$f_0 = f_n \equiv \frac{2n+1}{4d\cos\theta_2} c \equiv (n+\tfrac{1}{2})\Delta f , \tag{11b}$$

one will selectively excite this individual resonance. Equations (11a) and (11b) give

$$n_0 \gg 2n + 1, \tag{11c}$$

determining the required minimal length of the incident pulse

$$p_{inc}(x,z,t) = \int_{-\infty}^{\infty} G(k) e^{ik(x\sin\theta_3 - z\cos\theta_3 - c_3 t)} dk/2\pi . \tag{12a}$$

Using for the reflection coefficient in the reflected pulse,

$$p_{ref}(x,z,t) = \int_{-\infty}^{\infty} G(k) R(k) e^{ik(x\sin\theta_3 + z\cos\theta_3 - c_3 t)} dk/2\pi , \tag{12b}$$

the expression of Eq. (2a) rewritten as

$$R(k) = \sum_{m=0}^{\infty} D_m e^{imkD} \tag{13a}$$

with

$$\begin{aligned} D_0 &= -R_3 , \\ D_1 &= R_1(1 - R_3^2), \\ D_m &= D_1 (R_1 R_3)^{m-1}, \qquad m \geq 2. \end{aligned} \tag{13b}$$

Calling the observer's position (x_0, z_0) and using a time variable t_3 which vanishes when the leading edge of the reflected pulse reaches the observer, one finds

$$\begin{aligned} p_{ref}(x_0, z_0, t) = \sum_m D_m \Big\{ &\Theta\left(t_3 - \frac{mD}{c_3}\right) \sin\omega_0 \left(t_3 - \frac{mD}{c_3}\right) \\ &- \Theta\left(t_3 - t_p - \frac{mD}{c_3}\right) \sin\omega_0 \left(t_3 - t_p - \frac{mD}{c_3}\right) \Big\}, \end{aligned} \tag{14a}$$

where

$$\Theta(\tau) = \begin{cases} 0 & \tau < 0 \\ 1 & \tau \geq 0 \end{cases} \tag{14b}$$

is the Heaviside function. This corresponds to a series of overlapping wave trains whose outline is depicted in Fig. 4. The first rectangle outlines the specularly reflected pulse, the following ones the pulses that underwent (multiple) internal reflections. Since their coefficients D_m and D_{m+1} have equal signs for m=0 and opposite signs for $m > 0$, and since at every resonance the relative phase difference between any two successive sine functions in Eq. (14a) can be shown to be π, one sees that the individual wave trains are in phase with each other for $m > 0$, but are out of phase with the specular pulse (m=0).

For the example with layer parameters given by Eq. (3), and assuming normal incidence throughout, we evaluate numerically the reflected signal of Eq. (14a). The resonances spacing is $\Delta f \approx (1272/d)$Hz, with d measured in meters. We choose a spectral width $\Delta F = 0.1\Delta f$ so that $n_0 = 20 f_0/\Delta f$ and $t_p = 20/\Delta f$, and let the carrier frequency coincide with the third

resonance (n=2) so that fo = 2.5Δf. Figure 5 shows the reflected signal, starting at the receiver's time t_3=0. With the internally reflected components coming in at intervals of D/c_3 (here equal to 2.5 cycles of the carrier), the signal is step-wise reduced to its steady-state amplitude. After the passing of the trailing edge of the specular pulse at $t_3=t_p$, only the internally reflected pulses remain, manifesting themselves as a ringing of the selectively excited resonance.

If the carrier frequency is chosen halfway between two adjacent resonances, the results are as shown in Fig. 6 for a choice of $f_0=3.0\Delta f$. Successive internal reflections interfere destructively, causing the alternating steps in the initial transients leading to the steady-state amplitude. Some ringing is seen to persist even here (at a small amplitude level), since finite resonance widths cause some overlap in the resonance peaks.

Figure 7 shows the case of $f_0 = 2.6\Delta f$, i.e. the carrier frequency being slightly off-resonance (by 1/10 of the resonance spacing). The steady-state amplitude has already changed significantly compared to the on-resonance case of Fig. 5, indicating a narrow resonance width.

The half-width of the resonance peaks (which is here the same for all resonances, cf. Fig. 3) is related to the imaginary part of k_n^*, Eqs. (5), by

$$\frac{\gamma_n}{2} = \frac{c_3}{2\pi} |Im\, k_n^*| = \frac{1}{2\pi}\frac{c_3}{D} \ln\left(-\frac{1}{R_1 R_3}\right) \qquad (15a)$$

(case $R_1R_3<0$). Since $f_n = (n+\frac{1}{2})\Delta f$, we have

$$\frac{\gamma_n}{2} = \frac{\Delta f}{2\pi} \ln\left(-\frac{1}{R_1 R_3}\right). \qquad (15b)$$

The ringing, seen from Eq. (14a) and Fig. 5 to take place in a step-wise decaying fashion at the time intervals $\Delta t=1/\Delta f = D/c_3$:

$$p_{ref}(t = t_p + n\Delta t) = \frac{D_1}{(-R_1 R_3)^n}, \quad t > t_p, \qquad (16a)$$

may be approximated by a decaying exponential

$$p_{ref}(t=t_p+n\Delta t) \cong D_1 e^{-\gamma n \Delta t}, \qquad t > t_p. \tag{16b}$$

Comparison gives

$$\gamma = \Delta f \ln(-1/R_1 R_3), \tag{16c}$$

or

$$\gamma = \pi \gamma_n, \tag{16d}$$

which shows that the resonance half-width γ_n may be directly determined by measuring the decay content of the ringing. From Eq. (8a) it is apparent that the resonance spacing is larger for oblique incidence than from normal incidence (provided that $c_2 > c_3$, which is assumed). The resonance width as given by Eq. (15b) may, on the other hand, increase or decrease with the angle of incidence. However, the relative halfwidth (the halfwidth divided by the resonance spacing) always decreases, i.e. the resonances appear more pronounced for oblique incidence than for normal incidence.

4. Information Content of the Reflected Signal

For a steady-state incident signal, the only information obtained is that contained in the total reflection coefficient,

$$|R|^2 = \frac{R_1^2 + R_3^2 - 2R_1 R_3 \cos kD}{1 + R_1^2 R_3^2 - 2R_1 R_3 \cos kD}. \tag{17}$$

With a finite-length sinusoidal pulse train, however, one may measure separately the three quantities:

$$R_S = |R_3| \tag{18a}$$

(the amplitude of the specular reflection),

$$R_I = \frac{R_1 (1-R_3^2)}{(1+R_1^2 R_3^2 - 2R_1 R_3 \cos kD)^{1/2}} \tag{18b}$$

or, more conveniently,

$$R_I^{(1)} = R_1(1 - R_3^2) \tag{18b'}$$

(the amplitude of all internal reflections, or only of the first one, respectively), and

$$\Delta t = 1/\Delta f = c_3/D \tag{18c}$$

(the delay time between successive internal reflection). The measurement of R_I or $R_I^{(1)}$ can be seen to be equivalent to that of γ, cf. Eqs. (16). From our previous analytic expressions of these quantities, one may now derive three expressions that relate R_S, R_I and Δt to the layer parameters:

$$d\rho_2 = \frac{1-R_3}{1+R_3} \frac{Z_3}{2} \Delta t, \tag{19a}$$

$$\frac{1}{c_2^2} - \left(\frac{\Delta t}{2d}\right)^2 = \left(\frac{\sin\theta_3}{c_3}\right)^2, \tag{19b}$$

and

$$\left(\frac{R_{13} Z_3}{c_1}\right)^2 - \rho_1^2 = (R_{13}\rho_3)^2, \tag{19c}$$

where we defined

$$R_{13} = \frac{1-R_S^2 + R_I}{1-R_S^2 - R_I} \frac{1+R_S}{1-R_S}. \tag{19d}$$

This constitutes three equations, Eqs. (19a)-(19c), for the five unknowns c_1, c_2, ρ_1, ρ_2 and d of our ocean floor model. Information on the resonance order n, incidentally, is obtained from Eq. (11b), since the resonance spacing Δf is known from the measurement of Δt, Eq. (18c).

Two independent measurements of R_S, R_I and Δt at the same frequency, but at two different angles of incidence $\theta_3^{(1)}$ and $\theta_3^{(2)}$, can now be shown to lead to sufficient additional information so that one may solve the resulting equations for all bottom parameters involved. Indeed, Eq. (19b) then yields directly

$$d = \frac{c_3}{2}\left(\frac{\Delta t_2^2 - \Delta t_1^2}{\sin^2\theta_3^{(1)} - \sin^2\theta_3^{(2)}}\right)^{1/2}, \tag{20a}$$

$$c_2 = c_3\left(\frac{\Delta t_2^2 - \Delta t_1^2}{\Delta t_2^2 \sin^2\theta_3^{(1)} - \Delta t_1^2 \sin^2\theta_3^{(2)}}\right)^{1/2}, \tag{20b}$$

furnishing the unknowns d and c_2. With d known, Eq. (19a) can be used to find ρ_2.

Similarly, Eq. (19c) yields the remaining two unknowns,

$$c_1 = \left(\frac{(Z_3^{(1)} R_{13}^{(1)})^2 - (Z_3^{(2)} R_{13}^{(2)})^2}{R_{13}^{(1)2} - R_{13}^{(2)2}}\right)^{1/2}, \tag{20c}$$

$$\rho_1 = R_{13}^{(1)}\left[\left(Z_3^{(1)}/c_1\right)^2 - \rho_3^2\right]^{1/2}. \tag{20d}$$

In the above equations, Δt_1, $R_{13}^{(1)}$ and $Z_3^{(1)}$ are the values of Δt, R_{13} and Z_3 pertaining to the angles $\theta_3^{(1)}$, respectively. Thus, when long but finite sinusoidal sound pulses are used as probes, in principle only two

different measurements of R_S, R_I (or γ) and Δt have to be made at the same frequency and at two different angles, in order to deduce all unknown layer parameters.

5. Discussion

The acoustic resonance method for the remote sensing of ocean floor properties was introduced in our previous work [Nagl, Überall and Hoover, 1982] for the case of monochromatic, steady-state sinusoidal signals used as probes. In that case, resonances of ocean floor sediment layers, e.g., in frequency (or, alternately, in the angle of incidence) must be found by repeating the experiment at many different values of the frequency (or of the angle). With the present suggestion of using finite-length sinusoidal wave trains, the number of measurements can be dramatically reduced. The pulse length must be sufficiently great so that the specularly reflected amplitude and several of the signals multiply reflected from within a bottom layer overlap; it is then possible to selectively excite and study one individual resonance. The time delay between internal reflections determines the order of the resonance and the resonance spacing. Measurement of specularly and internally reflected amplitudes, or of the ringing of the resonance, carried out at two different angles then suffices in principle to furnish us with the values of the layer and substratum parameters, hence solving the inverse scattering problem. While all this was demonstrated here on the simple example of a fluid layer on top of a fluid substratum, it is to be expected that a multilayered ocean floor will in principle yield similar information due to layer resonances being set up

in individual layers by an incident finite-length wave train. Work on this problem is now in progress.

It should be noted that observations of the ringing of resonances, acoustically excited by finite-length wave trains, have been used [Maze, Taconet and Ripoche, 1981] in order to determine the resonance spectrum and the resonance widths of metal cylinders immersed in a fluid. These observations have been interpreted [Numrich et al., 1984] in terms of overlapping wave trains circumferentially propagating around the target, in a fashion similar to the multiply-reflected wave trains of the present paper. Likewise, overlapping wave trains in radar scattering have been analyzed analogously [Bowell and Überall, 1984].

Acknowledgements

This work was supported by the Office of Naval Research, U. S. Navy. We wish to thank Professor V. Klemas and Dean W. S. Gaither for their hospitality during the author's stay at the College for Marine Studies, University of Delaware. Useful discussions with Prof. R. E. Sheridan and Prof. F. Webster at that institution are acknowledged.

References

1. Bell, D. L., and W. J. Porter, Remote sediment classification potential of reflected acoustic signals, in Physics of Sound in Marine Sediments, Loyd Hampton (Ed.), Plenum Press, New York, 1974, pp. 319-336.
2. Hautz, R. E., Preliminary study of global sediment sound velocities from sonobuoy data, in Physics of Sound in Marine Sediments, Loyd Hampton (Ed.), Plenum Press, New York, 1974, pp.519-536.
3. Howell, W. E., and H. Überall, Selective observation of resonances via their ringing in transient radar scattering, IEEE Trans. Antennas Propagat., 1984 (submitted).
4. Maynard, G. L., G. H. Sutton, D. M. Hussong, and L. W. Kroenke, The seismic wide angle reflection method in the study of ocean sediment velocity structure, in Physics of Sound in Marine Sediments, Loyd Hampton (Ed.), Plenum Press, New York, 1974, pp. 89-118.
5. Maze, G., B. Taconet, and J. Ripoche, Influence des ondes de "Galerie à Echo" sur la diffusion d'une onde ultrasone plane par un cylindre, Physics Letters 84A (6), 309-312, 1981.
6. Nagl, A., H. Überall, and W. R. Hoover, Resonances in acoustic bottom reflection and their relation to the ocean bottom properties, IEEE Trans. Geosc. Remote Sens., GE-20(3), 332-337, 1982.
7. Numrich, S. K., W. E. Howell, H. Überall, and J. V. Subrahmanyam, Selective observation of elastic body resonances by using long pulses to excite a ringing response, J. Acoust. Soc. Amer., 1984 (submitted).

Figure Captions

Fig. 1. Geometry of the three-fluid model for an ocean floor with a sediment layer.

Fig. 2. Geometrical view of multiple-reflection decomposition for the reflection coefficient of a sediment layer.

Fig. 3. Plot of $|R(k)|^2$ vs. frequency-thickness fd, at normal incidence ($\theta_3 = 0^\circ$), showing (anti)resonances.

Fig. 4. Amplitudes of reflected overlapping wave trains.

Fig. 5. Reflected signal vs. time, for the carrier frequency coinciding with third resonance frequency. Layer parameters of Eq. (3).

Fig. 6. Reflected signal, for the carrier frequency halfway between the third and the fourth resonance frequency.

Fig. 7. Reflected signal, for the carrier frequency lying above the third resonance frequency by 1/10 of the resonance spacing.

FIG. 1

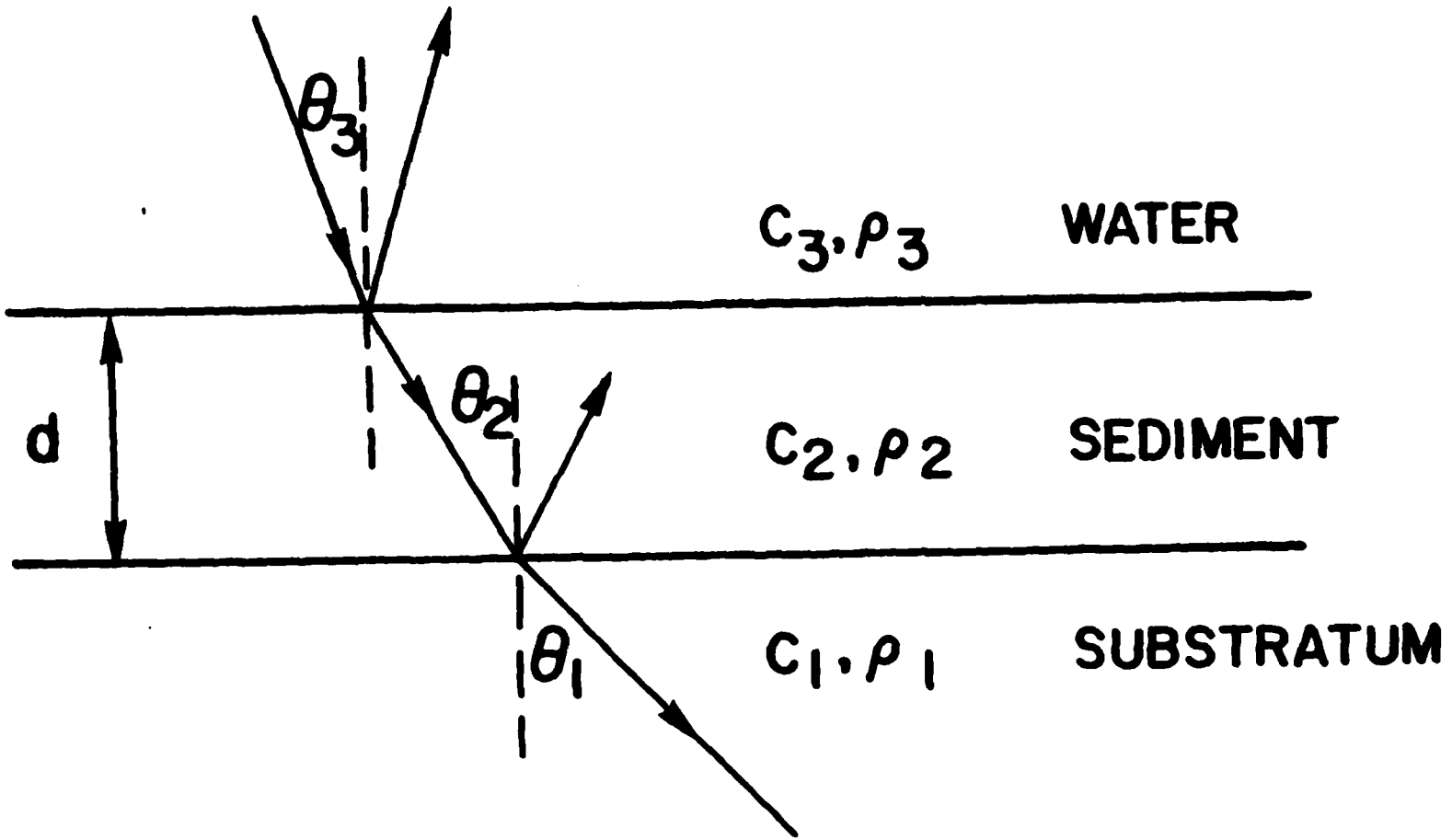
θ_3
C_3, ρ_3
WATER
d
θ_2
C_2, ρ_2
SEDIMENT
θ_1
C_1, ρ_1
SUBSTRATUM

FIG. 2

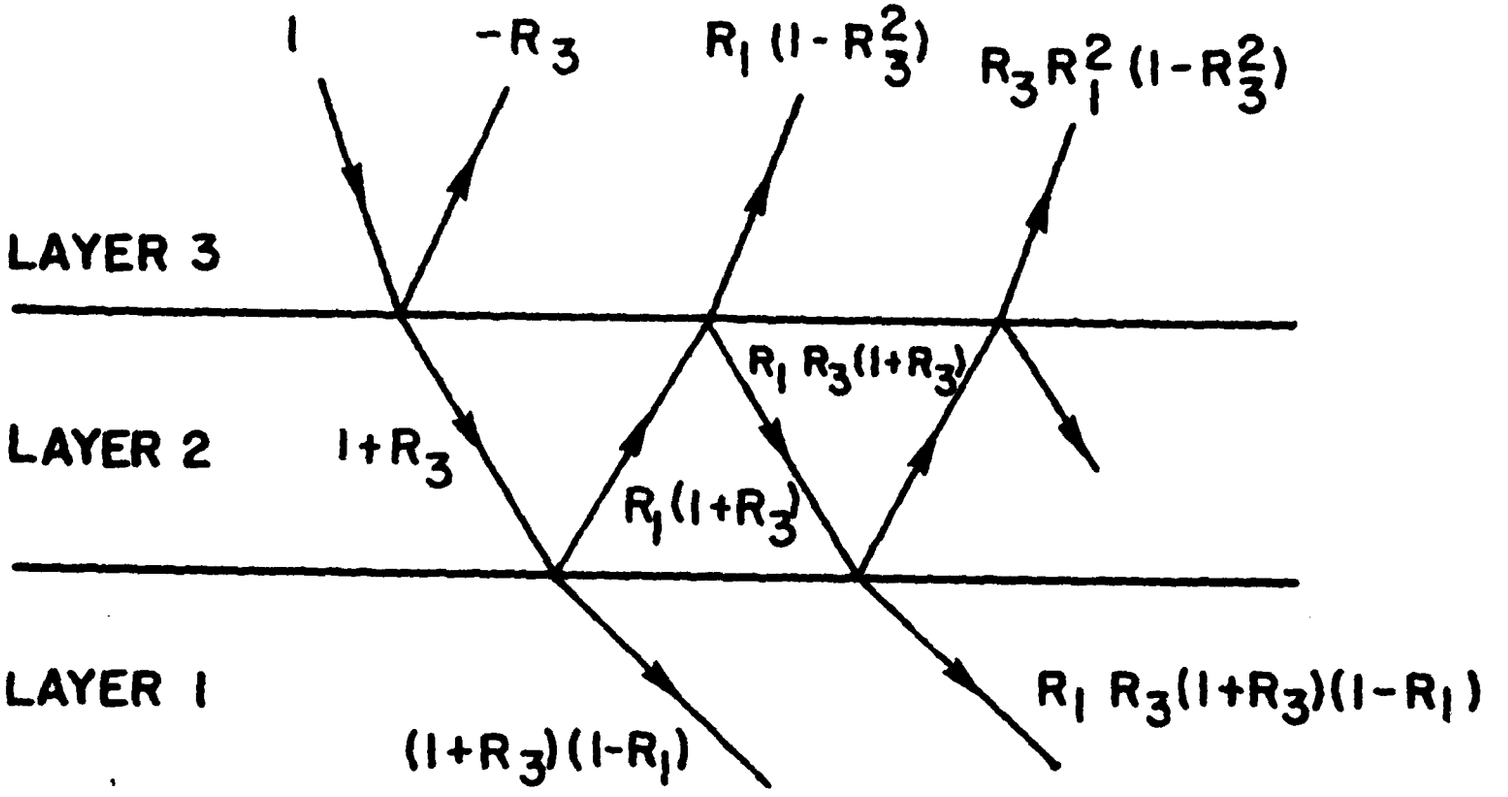
1
$-R_3$
$R_1(1-R_3^2)$
$R_3R_1^2(1-R_3^2)$
LAYER 3
$R_1R_3(1+R_3)$
LAYER 2
$1+R_3$
$R_1(1+R_3)$
LAYER 1
$(1+R_3)(1-R_1)$
$R_1R_3(1+R_3)(1-R_1)$

FIG. 3

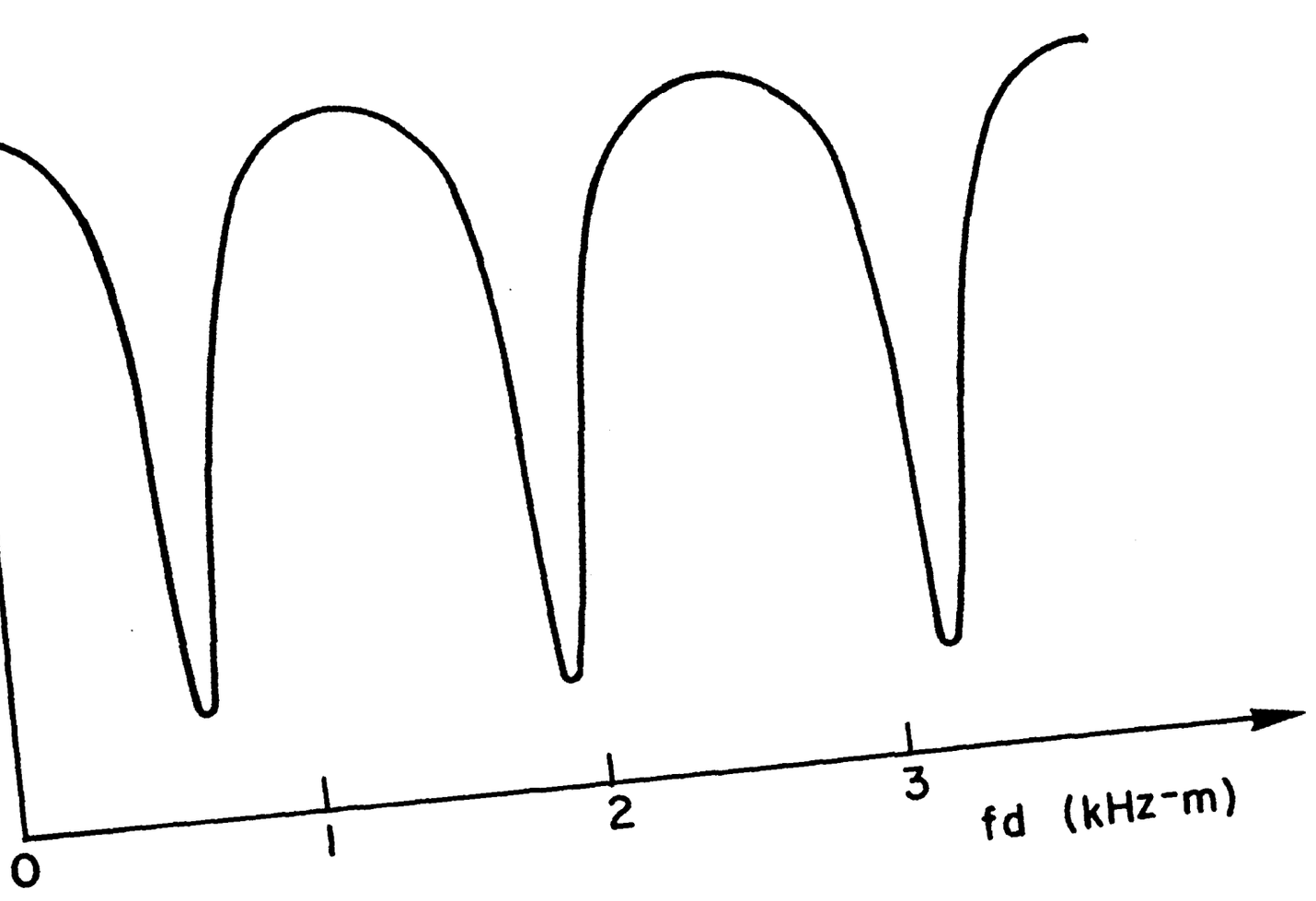

FIG. 4

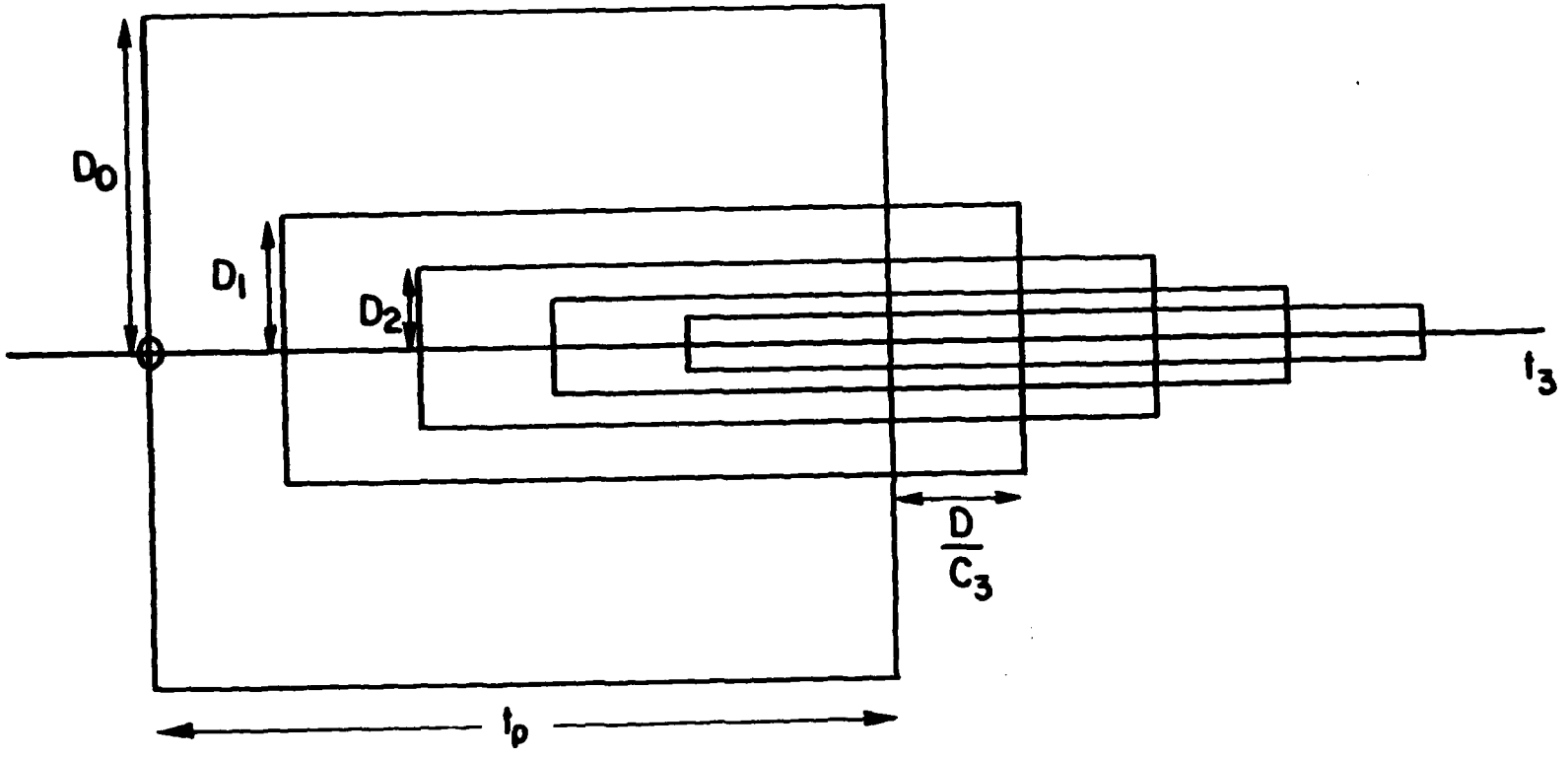

FIG. 5

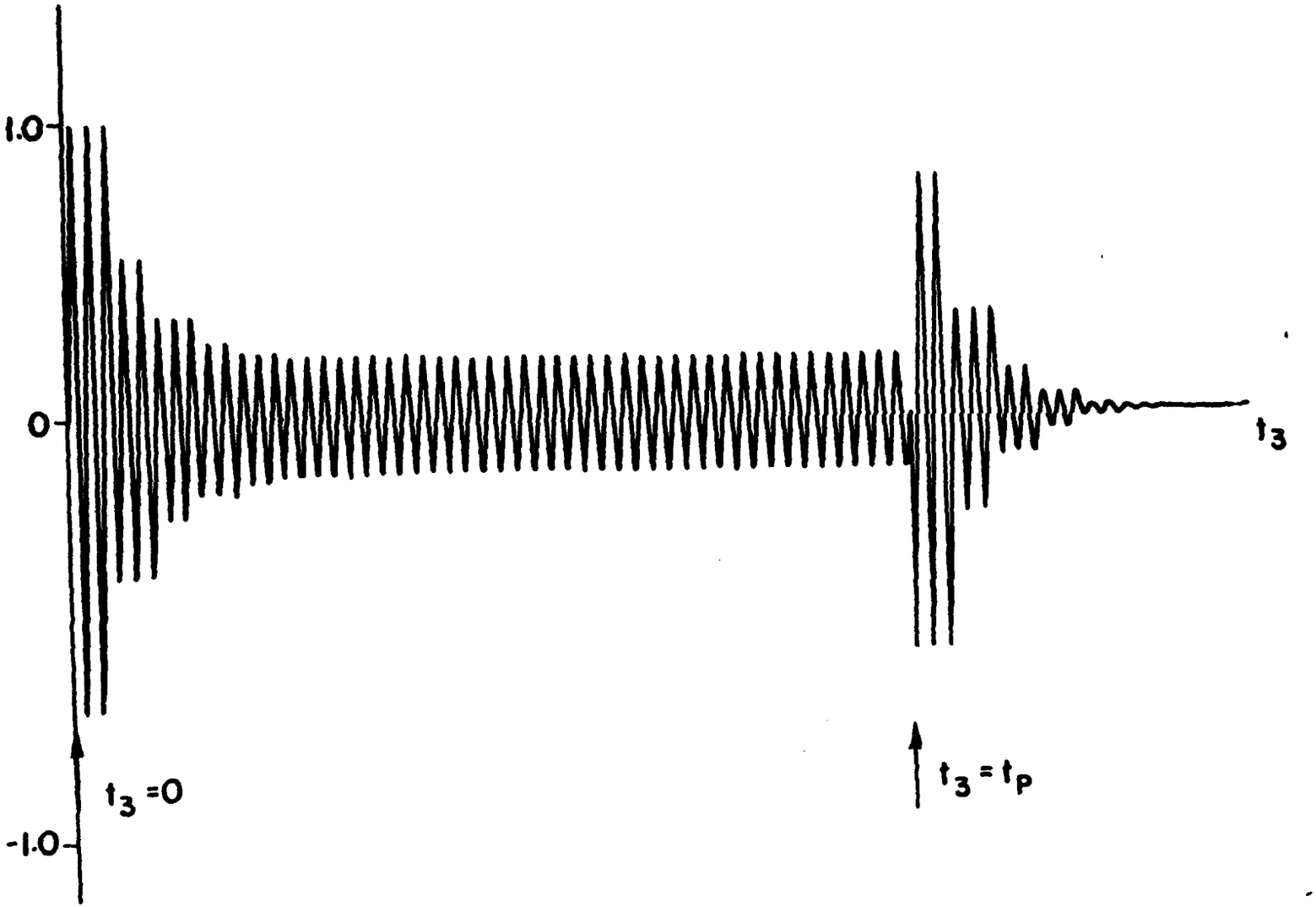

FIG. 6

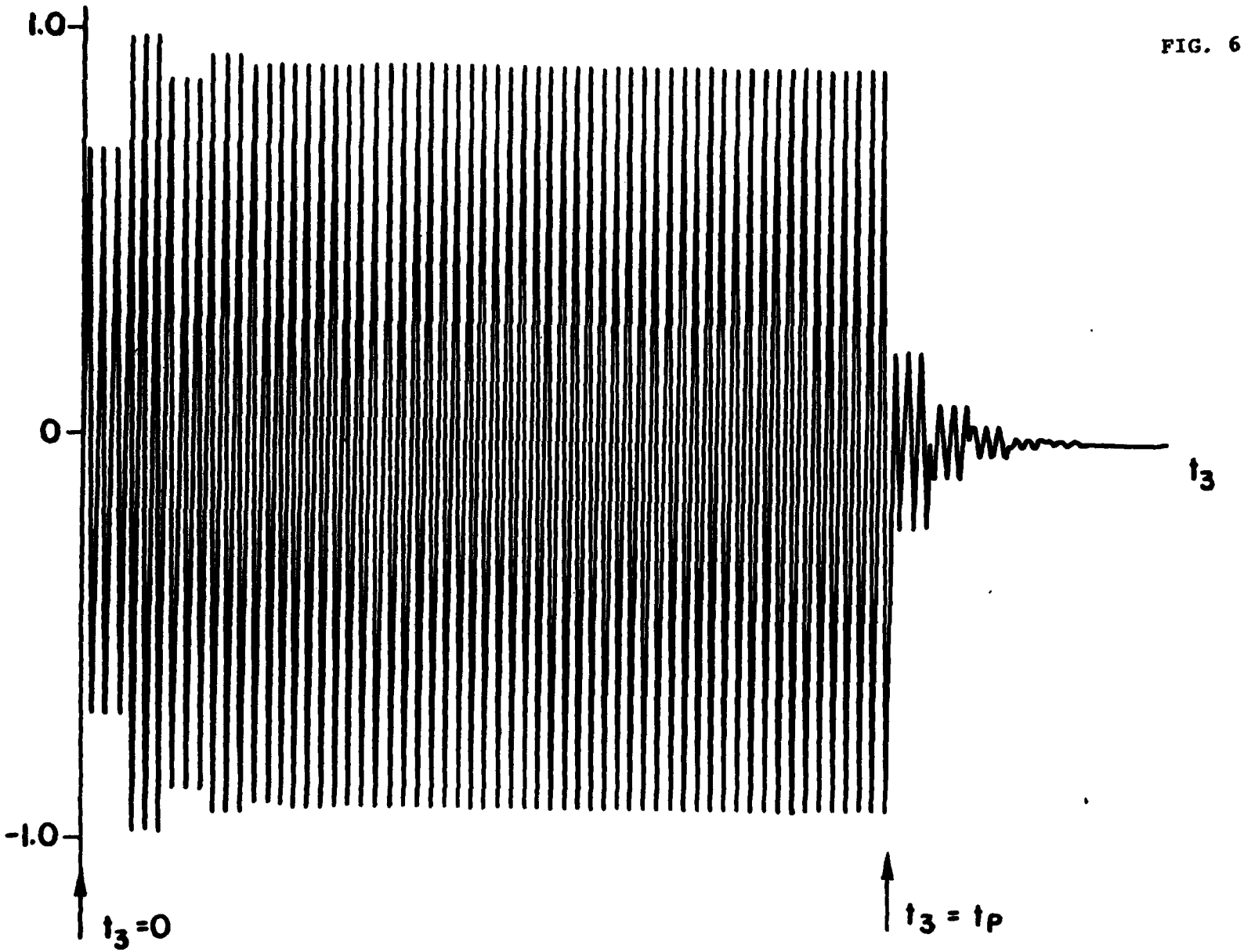

FIG. 7

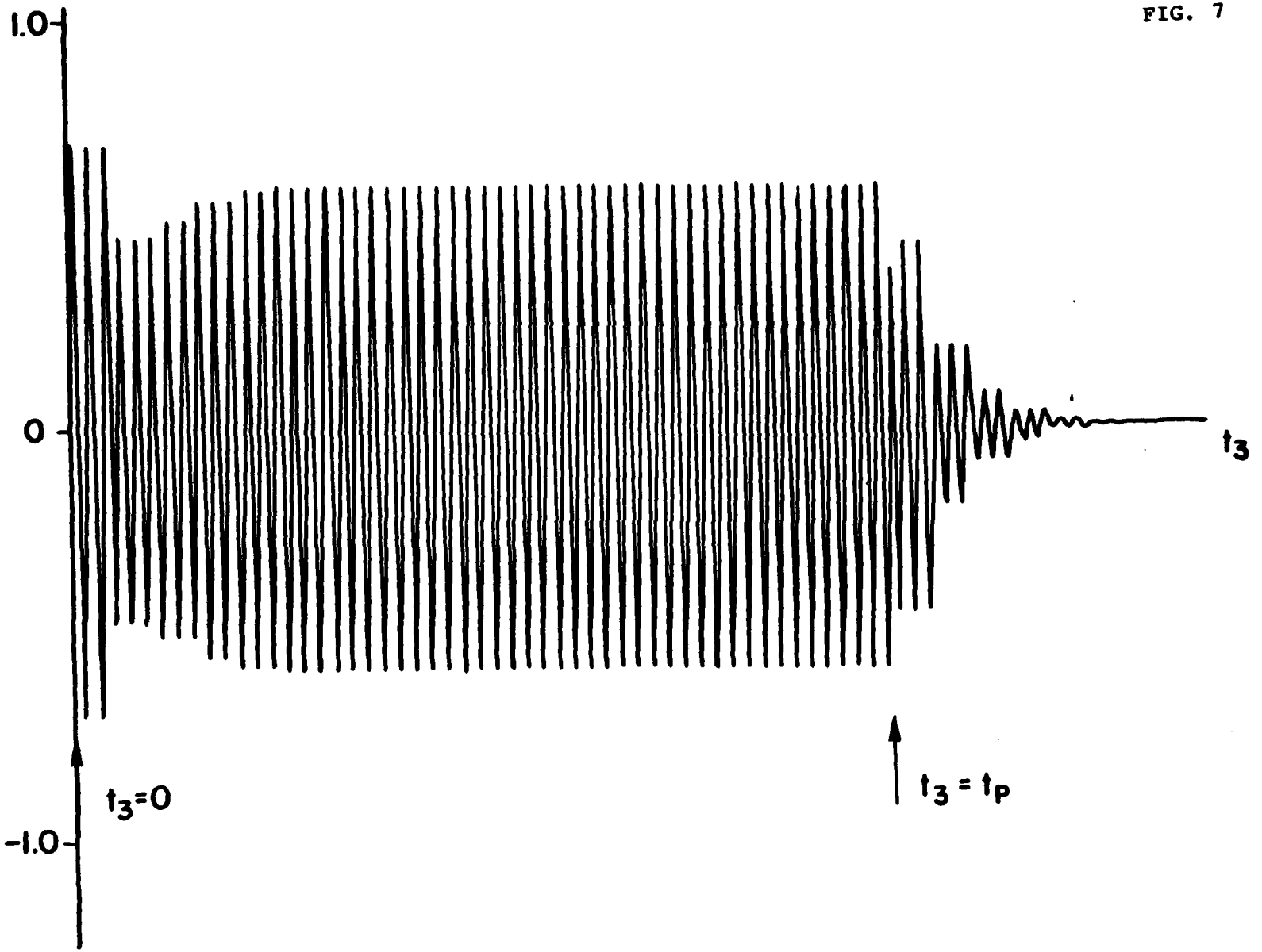

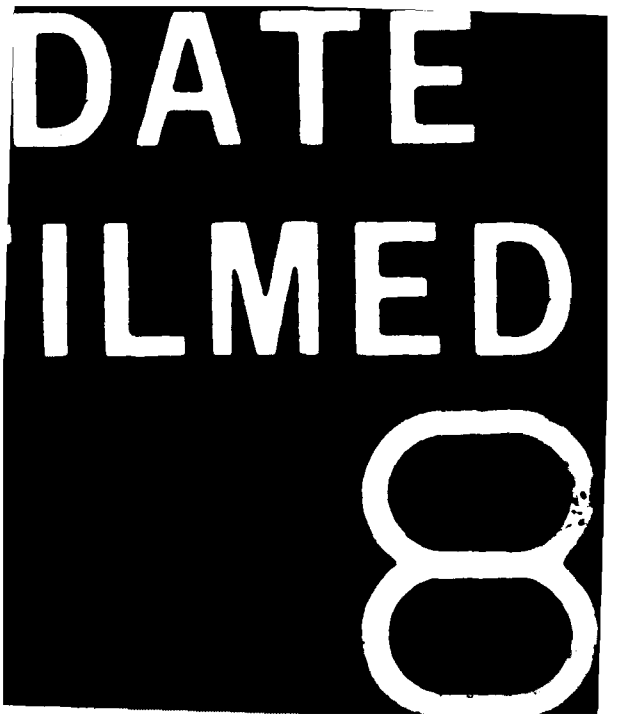
DATE
ILMED
8